NANO LETTERS

pubs.acs.org/NanoLett Letter

Refractive Index Modulation in Monolayer Molybdenum Diselenide

Melissa Li, Souvik Biswas, Claudio U. Hail, and Harry A. Atwater*

Cite This: https://doi.org/10.1021/acs.nanolett.1c02199 Read Online

ACCESS | Metrics & More | Article Recommendations | Supporting Information

ABSTRACT: Two-dimensional transition metal dichalcogenides are promising candidates for ultrathin light modulators due to their highly tunable excitonic resonances at visible and near-infrared wavelengths. At cryogenic temperatures, large excitonic reflectivity in monolayer molybdenum diselenide ($MoSe_2$) has been shown, but the permittivity and index modulation have not been studied. Here, we demonstrate large gate-tunability of complex refractive index in monolayer $MoSe_2$ by Fermi level modulation and study the doping dependence of the A and B excitonic resonances for temperatures between 4 and 150 K. By tuning the charge density, we observe both temperature- and carrier-dependent epsilon-near-zero response in the permittivity and transition from metallic to dielectric near the A exciton energy. We attribute the dynamic control of the refractive index to the interplay between radiative and non-radiative decay channels that are tuned upon gating. Our results suggest the potential of monolayer $MoSe_2$ as an active material for emerging photonics applications.

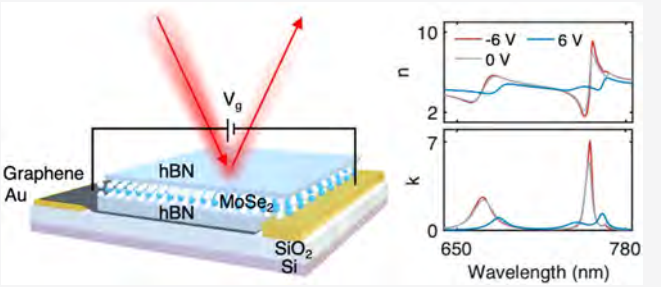

KEYWORDS: *2D materials, transition metal dichalcogenides, monolayer semiconductor, optical modulator, tunable optical properties, photonics*

INTRODUCTION

Two-dimensional (2D) materials have attracted a great deal of attention over the past decade due to the new physics that emerges as the materials transition from bulk to monolayer.[1,2] Particularly, transition metal dichalcogenides (TMDCs) such as $MoSe_2$ exhibit fundamentally distinct electronic and optical properties as the material evolves from indirect to direct band gap in the monolayer limit. As a result, the optical response of TMDC monolayers is dominated by strong excitonic resonances,[3−5] which are highly tunable with external electric field or doping,[6,7] dielectric environment engineering,[6,8] and strain.[9,10]

Recently, there has been considerable interest in studying active nanophotonic structures by combining tunable materials with resonant structures such as Mie resonators and phase gradient metasurfaces.[11−16] The ability to dynamically tune the complex index of an active material in metasurfaces enables comprehensive control of the scattered wavefront. For example, transparent conducting oxide-based metasurfaces have demonstrated electrically tunable amplitude and phase modulation of reflected light.[17−19] However, these devices operate at wavelengths above 1500 nm, which limits their applications to short-wavelength infrared (SWIR) optoelectronics. Extending the operating wavelengths to the visible range enables new applications to digital holography, imaging, cloaking, and virtual reality. 2D transition metal dichalcogenides are promising candidates for visible and near-infrared (NIR) light modulators due to their strong tunable excitonic resonances in the visible and NIR spectral range. The suppression of the excitonic response has previously been shown to modulate the refractive index of WS_2 at room temperature, but the non-radiative broadening at room temperature limits the achievable tunability.[20] By encapsulating TMDCs with hexagonal boron nitride (hBN) to produce high-quality heterostructures and operating at cryogenic temperatures, the excitonic line widths can be narrowed by over an order of magnitude.[21−24]

Here, we study the optical response of monolayer $MoSe_2$ at different carrier densities and cryogenic temperatures. Compared to other TMDCs, the optical properties of $MoSe_2$ at low temperatures have significantly less contributions from defects, allowing more accurate characterization of changes in the optical response. We exploit the narrow line widths of the excitons at low temperatures and show that Fermi level control via electrical gating of carrier density gives rise to large refractive index modulation at both the A exciton and B exciton energies. At temperatures between 4 and 150 K, we observe an epsilon-near-zero (ENZ)-like regime and hence a transition from metallic to dielectric near the A exciton energy, resulting in large changes in reflectance amplitude and phase. We note that while the temperature- and voltage-dependent

Received: June 4, 2021
Revised: August 28, 2021

https://doi.org/10.1021/acs.nanolett.1c02199
Nano Lett. XXXX, XXX, XXX−XXX

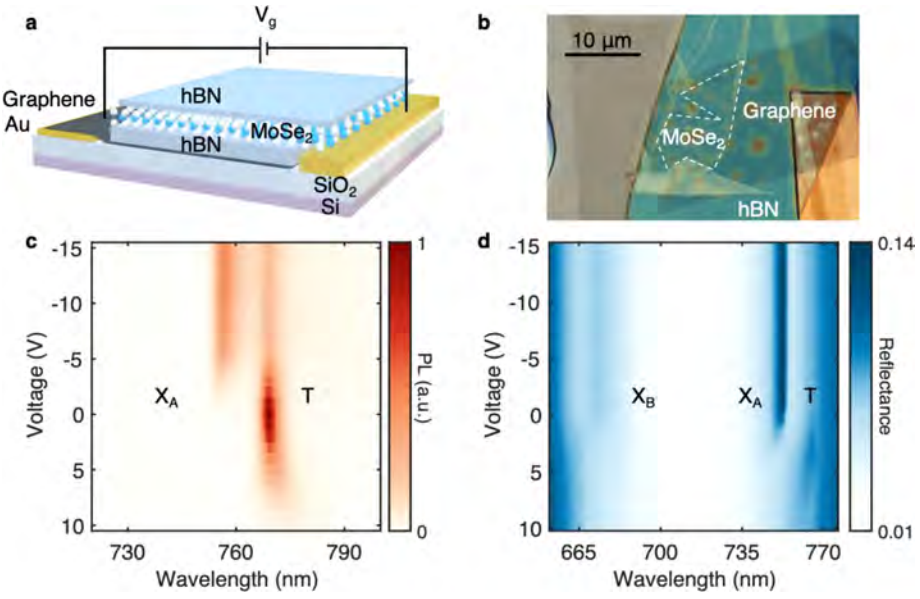

Figure 1. Electro-optic characterization of $MoSe_2$ heterostructure at T = 4 K. (a) Schematic of heterostructure. Carrier density in $MoSe_2$ is tuned by applying a voltage V_g across the bottom hBN. (b) Optical microscope image of the device, with the monolayer region enclosed in dashed lines. (c) Gate-dependent PL spectrum upon excitation with a 532 nm laser, showing two distinct peaks corresponding to the A exciton (X_A) and trion (T). (d) Gate-dependent reflectance spectrum obtained on the same device with three peaks corresponding to the A exciton (X_A), B exciton (X_B), and trion (T). The change in PL and reflectance can be observed in the electron-doped regime (positive voltages). To obtain the reflectance, we normalize the reflected intensity to the measured reflectance of a gold electrode.

reflectances have been previously shown,[24,25] the gate-tunability of the complex refractive index has not been studied in these TMDCs at cryogenic temperatures. In applications where electro-optic modulation is used to tune the scattering response of nanophotonic structures near excitonic and geometrical resonances, it is important to characterize the complex refractive index changes accompanying the observed reflectance modulation.[26,27] Our demonstration of refractive index tunability indicates the possibility to manipulate light with monolayer 2D materials for ultra-thin optical modulators.

RESULTS

We measure the gate-dependent reflectance spectra of a monolayer $MoSe_2$ device at cryogenic temperatures using a broadband white light source. The schematic and microscope images of the device are shown in Figure 1a,b. The device consists of an $MoSe_2$ monolayer encapsulated between top hBN (5.2 nm) and bottom hBN (25 nm), which passivates the $MoSe_2$ monolayer to enhance the carrier mobility and reduces the line width.[21−23,28] A bottom few-layer graphene flake serves as the back electrode to control the carrier density in the $MoSe_2$. The entire heterostructure, fabricated with an all-dry transfer technique, is placed on an SiO_2/Si substrate with pre-patterned gold electrodes to contact the $MoSe_2$ and graphene. The carrier density in $MoSe_2$ is tuned by applying a gate voltage across the bottom hBN, which acts as the capacitor between the graphene and $MoSe_2$. To obtain the absolute reflectance of the TMDC heterostructure, the spectrum is normalized to that of an optically thick gold layer adjacent to the sample.

The gate-dependent excitonic features of $MoSe_2$ are shown in both photoluminescence (PL) and reflectance spectra in Figure 1c,d. At 4 K, we observe two main features in PL that are associated with the A exciton and trion resonances at wavelengths of 757 and 769 nm, respectively. However, in reflectance, we observe three features associated with the A exciton, trion, and B exciton resonances. The presence of A and B excitons is attributable to the spin−orbit coupling induced valence and conduction band splitting.[29] We note that our PL spectrum does not contain a prominent B exciton feature, presumably because the PL quantum yield is lower than that of the A exciton. Moreover, we observe two main differences in the trion features when comparing the PL and reflectance measurements. First, at 0 V, we observe a stronger PL signal from the trion compared to the A exciton, whereas in reflectance, the A exciton feature is dominant. This difference is commonly seen at 4 K in $MoSe_2$ and can be explained by the low oscillator strength of trions.[30,31] While the oscillator strength of a transition is intimately related to the radiative lifetime and PL intensity, the one-to-one correspondence is not typically observed due to the band structure and additional relaxation channels. The trion exists at a lower energy than the A and B excitons, and the PL emission favors the lowest energy state. Therefore, even though the trion has low oscillator strength and, hence, low absorption, when the sample is excited above the A and B exciton energies with a 532 nm laser, we see a strong trion PL contribution from the relaxed A and B exciton states.

Furthermore, we observe a difference in the energy shift direction of the trion when the sample is electron doped, which corresponds to positive voltages in our electrostatic gating scheme. In reflectance, we see that the peak energy of the trion feature blueshifts, but in PL, the peak energy redshifts. To understand this finding, we consider the different mechanisms that can influence the reflectance and PL spectra.[32−34] Reflection can be affected by Pauli blocking upon doping, leading to an increase in the effective optical gap which results in a blueshift. However, PL involves recombination of electron−hole pairs that relax to the band edges, resulting in the Stokes shift which increases with doping.[29]

https://doi.org/10.1021/acs.nanolett.1c02199
Nano Lett. XXXX, XXX, XXX−XXX

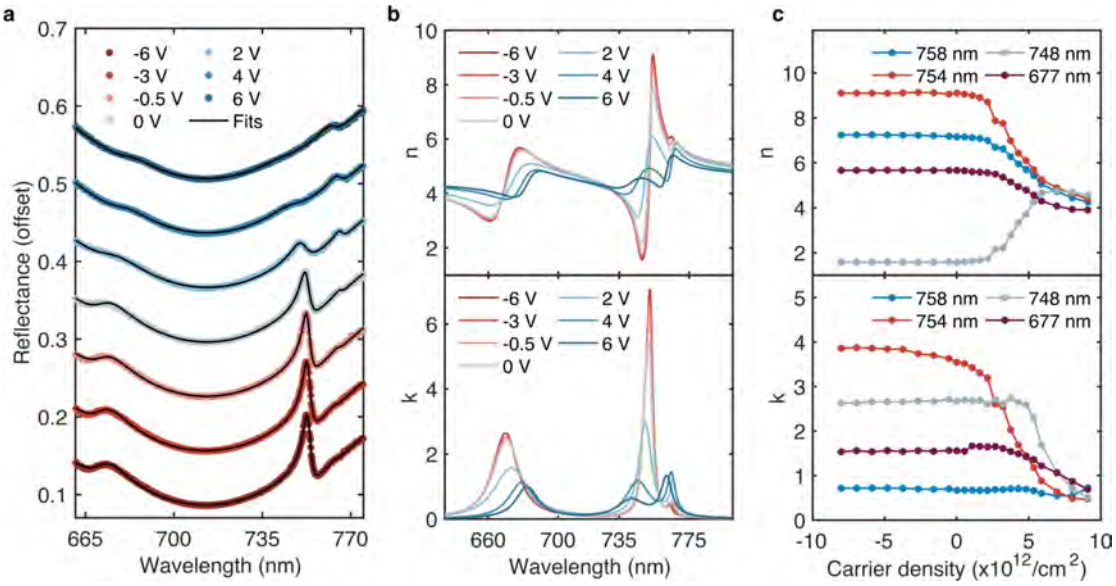

Figure 2. Gate-dependent reflectance spectra and refractive index at T = 4 K. (a) Reflectance spectra of monolayer $MoSe_2$ at 4 K for different gate voltages. The colored points are experimental data from line cuts of different voltages from Figure 1d. The solid black lines are fits from transfer matrix calculations where the $MoSe_2$ dielectric function is modeled using the multi-Lorentzian model. The spectrum corresponding to −6 V shows the absolute reflectance values, and the spectra at higher voltages are offset for clarity. (b) Fitted real (n) and imaginary (k) parts of the refractive index with different voltages. (c) Changes in the real and imaginary parts as a function of electron carrier density for four different wavelengths.

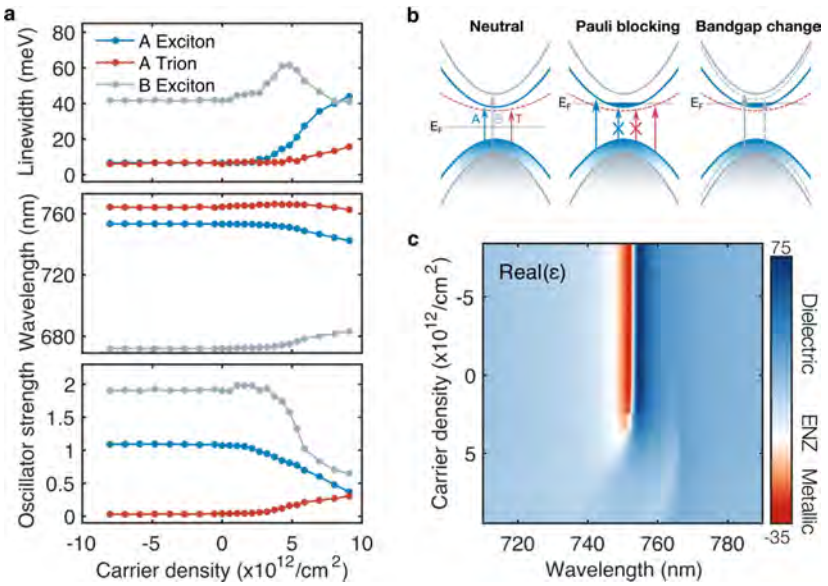

Figure 3. Gate-tunability of exciton parameters and ENZ response at T = 4 K. (a) Change in oscillator strength, resonance wavelength, and oscillator line width for the A exciton, B exciton, and trion as a function of electron carrier density. (b) Schematic of electronic band structure, allowed transitions, and competing electronic effects for different Fermi levels. (c) Real part of the dielectric permittivity as a function of wavelength and carrier concentration. Near the A exciton resonance (754 nm), the $MoSe_2$ undergoes a transition from optically metallic to optically dielectric.

Another possible explanation for this difference in the energy shifts in PL and reflectance is that the quasiparticle associated with the lower energy peak is potentially an attractive polaron instead of a trion.[30,35] However, here, we will refer to the lower energy feature as the trion for consistency.

We obtain the complex refractive index for $MoSe_2$ by using a Kramers−Kronig consistent analysis and fitting the reflectance spectra of our entire heterostructure stack with the transfer matrix method to account for interference effects. We begin our analysis by modeling the dielectric function of the monolayer as a sum of Lorentz oscillators:[36]

$$\tilde{\epsilon} = \epsilon_1 + i\epsilon_2 = \epsilon_\infty + \sum_j \frac{f_j}{E_j^2 - E^2 - iE\gamma_j} \quad (1)$$

Here ϵ_∞ is the background $MoSe_2$ dielectric constant and f_j, E_j, and γ_j are the oscillator strength, resonant energy, and line width of the jth oscillator, respectively. In our analysis, each oscillator represents an individual excitonic or trionic feature. The complex refractive index is then calculated from the fitted dielectric function as follows: $\tilde{n} = n + ik = \sqrt{\tilde{\epsilon}}$. We note that this method of obtaining the refractive index has been previously demonstrated to give accurate results for TMDC

https://doi.org/10.1021/acs.nanolett.1c02199
Nano Lett. XXXX, XXX, XXX−XXX

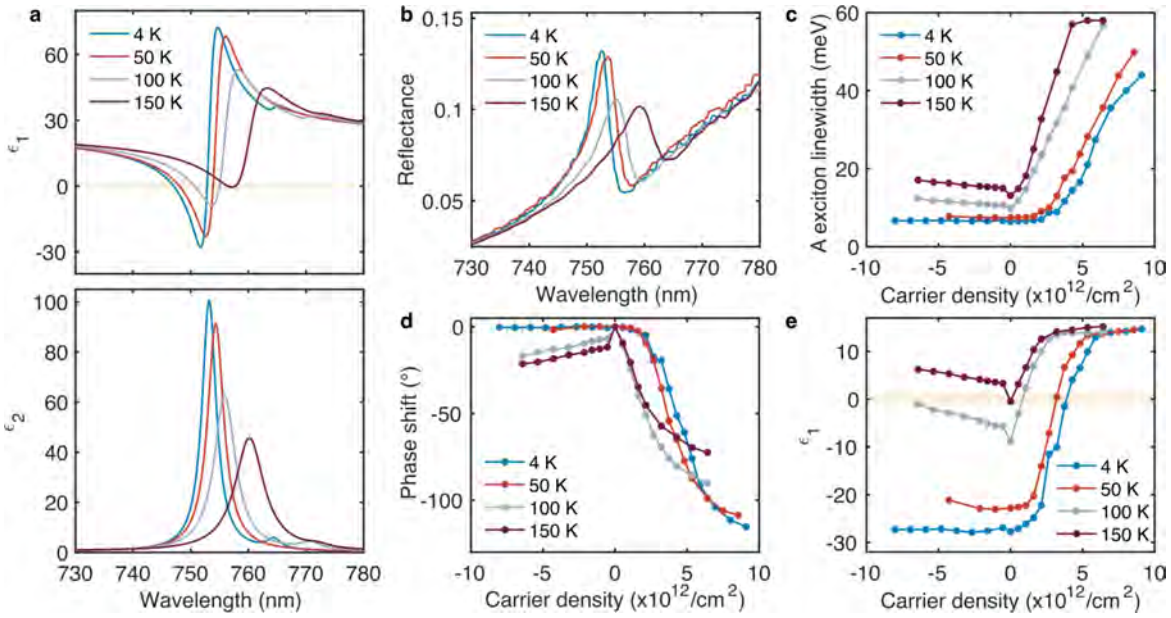

Figure 4. Gate dependence of dielectric function and phase change at different temperatures. (a) Temperature-dependent real and imaginary parts of the dielectric function near the A exciton at charge neutrality for each temperature. (b) Measured temperature-dependent reflectance spectra at charge neutrality. (c) Carrier-dependent A exciton line width for different temperatures. (d) Carrier-dependent change in phase of the reflected light from the charge-neutral point for different temperatures. (e) Minimum value of the real part of the dielectric permittivity near the A exciton resonance for different carrier densities and temperatures. The shaded region shows the ENZ regime.

monolayers from reflectance measurements at room temperature.[36] In Figure 2a, we see three prominent asymmetric features in the reflectance that exhibit a local minimum and maximum near the A exciton, trion, and B exciton resonances. At 4 K, the line widths of these three oscillators are much narrower than their line widths at room temperature.[24,36] Thus, their oscillator contribution dominates, and we can approximate the dielectric function as a sum of these three oscillators, since the resonance features from the other oscillators associated with the A2s and A3s states are not observed in our measurements. To account for oscillators outside of our measurement window, we add a background dielectric constant, $\epsilon_\infty = 20$, which is an intrinsic property that depends on all the higher energy optical resonances of the material.[36]

The gate-dependent real and imaginary parts of the refractive index are shown in Figure 2b. By comparing the experimental results with the corresponding fitted gate-dependent reflectance, we see that modeling the $MoSe_2$ dielectric function with three oscillators yields an excellent fit to the data (Figure 2a). The refractive index near both the A exciton and B exciton energies shows extremely large gate tunability. At 748 and 754 nm, both the real and imaginary parts can be tuned by over 200% compared to their values at the charge-neutral point, where the gate voltage $V = -2.5$ V maximizes the exciton signal (Figure 2c). We note that this refractive index modulation is over 5 times larger than previously reported for both the real and imaginary parts in TMDCs.[20]

To better understand the mechanisms for the large refractive index modulation, we study the effects of carrier density on the oscillator strength, line width, and peak energy of the three oscillators. The resulting fitting parameters for each oscillator as a function of carrier density are shown in Figure 3a. For negative voltages, the changes in the oscillator strength, line width, and peak energy are negligible since the hole doping is less efficient and presumably the semiconductor resides in a more "intrinsic" regime. However, for electron doping, we see an exchange of oscillator strengths between the A exciton and trion and a reduction in the oscillator strengths for both the A and B excitonic features. For the line width and peak energy behaviors, the A exciton and trion features are noticeably different from the B exciton feature. Figure 3a shows that the line widths of the A exciton and trion both broaden monotonically with carrier density, while the B exciton initially broadens up to a certain doping density and then narrows. Moreover, the peak energies for both the A exciton and trion blueshift, while that for the B exciton redshifts.

The striking differences in line width variation and energy shifts can be explained by considering the electronic band structure of $MoSe_2$ along with the effects of Coulomb scattering, screening, and Pauli blocking (Figure 3b). First, the screening of the electric field due to increased free carriers reduces the strength of the Coulomb interaction for the exciton. This leads to an overall decrease in the oscillator strength for both the A exciton and B exciton, attributable to a reduction in the binding energy. We note that while the trion oscillator strength increases due to a higher probability of formation in the presence of excess charges, the overall sum of A exciton and trion oscillator strengths decreases, which is consistent with the effects of screening and reduced Coulomb interactions. Second, for the A exciton and trion, the Coulomb scattering leads to a decrease in the coherence lifetime, resulting in spectral broadening of both transitions. The behavior at the B exciton energy is likely due to an emergence of charged B excitons at low electron densities, where the total line width initially broadens due to contributions from both the neutral and charged B excitons. At higher electron densities, the neutral exciton vanishes, leading to a decrease in the total line width. However, the energies of the neutral and charged B excitons are close and are not spectrally resolved in the measurements, so only the combined contribution is

https://doi.org/10.1021/acs.nanolett.1c02199
Nano Lett. XXXX, XXX, XXX−XXX

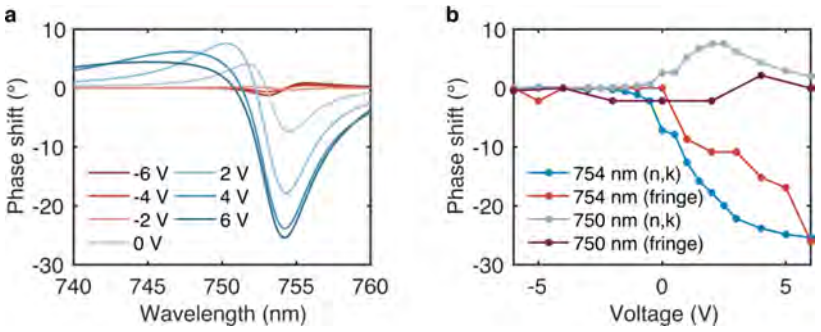

Figure 5. Change in phase as a function of wavelength and voltage for 4 K. (a) Calculated phase shift spectra from $V = -2.5$ V using extracted n, k values around the A exciton energy. (b) Comparison between calculated phase shift from n, k and measured phase shift from fringe shift measurements for 754 and 750 nm.

considered in Figure 3a.[29] Finally, Pauli blocking typically leads to a decrease in the binding energy due to the occupation of electronic states and the fermionic nature of electrons. Therefore, when the Fermi level is between the conduction bands, the A exciton and trion features will blueshift. However, the B excitons are only influenced by screening effects, which lead to redshifts from the re-normalization of the bandgap to lower energies.

Next, we explore the tunability of the ENZ and negative ϵ_1 behavior of $MoSe_2$ at low temperatures. We note that, in previous reports of gate-dependent index modulation in TMDCs, the real parts of the dielectric functions have been strictly positive,[20,37] and the negative permittivity and ENZ properties in $MoSe_2$ have not been examined or observed in either monolayer or multilayer $MoSe_2$.[36,38] In Figure 3c, we observe that, near the A exciton resonance, the real part of the dielectric function becomes negative when the sample is hole doped or nearly intrinsic. As the electron density increases, the dielectric function approaches the ENZ regime and becomes positive over the entire spectral range. Moreover, we observe a spectral shift of the ENZ regime that results from the blueshift of the A exciton resonance.

Whether ϵ_1 takes positive or negative values can be attributed to three main factors. As mentioned previously, the first attribute is the background dielectric constant (ϵ_∞) that shifts ϵ_1 to a higher positive value. This is primarily dependent on the bulk properties of $MoSe_2$ and does not depend on the A exciton properties. The second and third factors are the oscillator strength and the line width of the exciton resonance, where larger oscillator strengths and narrower line widths result in a significant increase in ϵ_2 and allow ϵ_1 to become negative. This can be shown through comparing the carrier-density-dependent exciton properties in Figure 3a with the corresponding ϵ_1 in Figure 3c. When the electron density reaches around $4 \times 10^{12}/cm^2$, the A exciton oscillator strength noticeably decreases and the line width broadens, which also corresponds to the doping density where ϵ_1 becomes positive.

We perform the same gate-dependent measurements and analyses at higher temperatures of 50, 100, and 150 K (Figures S1−S5). The temperature-dependent real and imaginary parts of the dielectric function and the corresponding reflectance spectra at the charge neutral point are shown in Figure 4a,b, respectively. While the increase in temperature allows for an additional line width broadening mechanism, even at these higher temperatures, ϵ_1 can attain negative values if the A exciton line width is around 13.2 meV or lower (Figure 4c). At 150 K, the line width is around 13.1 meV at charge neutrality, corresponding to a small negative value of $\epsilon_1 = -0.4$. Furthermore, by comparing Figure 4c and Figure 4e, we see that, at each temperature, the carrier density that gives rise to line widths broader than 13.2 meV also corresponds to the carrier density where ϵ_1 crosses the ENZ regime and switches from negative to positive.

From the gate-dependent change in the complex refractive index, we calculate the corresponding change in the phase of the reflected light off an isolated monolayer $MoSe_2$. The resulting phase modulations as functions of wavelength, voltage, and temperature are shown in Figures 4d and S6. We observe the largest overall change in the phase at 4 K, where $\Delta\Phi = 115°$. We attribute this large tunability as a result of the narrower line widths at lower temperatures, which gives rise to a larger refractive index change around the resonance energies.

As a proof-of-concept demonstration of phase modulation, we directly measure the phase shift of the reflected light under applied bias by using an interferometer measurement where the laser light illuminates the edge of our monolayer flake. Therefore, a portion of the incident beam is reflected from the monolayer flake, while another portion is reflected from the substrate, which acts as a built-in phase reference. We then fit intensity profiles obtained from the images of the recorded interference fringes to sinusoidal functions, as shown in Figure S11, and calculate the relative displacement of the interference fringes originating from the sample and the back reflector reference with applied bias. Our measured phase shifts obtained directly from fringe shift measurements are in good agreement with the phase shift extracted from the refractive index values at wavelengths corresponding to both the excitonic resonance and off resonance (Figure 5a,b). At 754 nm, where the change in refractive index is maximal, we observe over a 25° phase shift. We note this phase shift is observed in the absence of coupling to antennas or cavities, which is an important quantity for applications such as active metasurfaces.[18,19,39] By integration of gated monolayer $MoSe_2$ with a cavity or metasurface, we find that the phase shift can be increased to over >270°, as illustrated in Figure S12.

So far, we have considered how the oscillator strength and line width change as a function of carrier density and temperature. However, these parameters can be directly related to the radiative γ_r and non-radiative decay rates γ_{nr} of the excitons by rewriting the dielectric function to take the form[24]

https://doi.org/10.1021/acs.nanolett.1c02199
Nano Lett. XXXX, XXX, XXX−XXX

$$\epsilon = \epsilon_1 + i\epsilon_2 = \epsilon_\infty - \frac{\hbar c}{d_{MoSe_2}} \sum_j \frac{\hbar\gamma_{r,j}}{E_j(E - E_j - i\hbar\gamma_{nr,j}/2)} \quad (2)$$

In Figure S7, we plot the extracted radiative and non-radiative decay rates as functions of carrier density as well as temperature. At 4 K, the line width resulting from the radiative rate of the A exciton is extremely narrow, corresponding to a radiative line width of 1.8 meV. When the $MoSe_2$ is intrinsic, the total decay rate of the A exciton, $\gamma_T = \gamma_r + \gamma_{nr}$, is around 6 meV, which is in good agreement with a Voigt-like line profile of the A exciton PL (Figure S8). As both the temperature and the carrier density increase, the non-radiative line width broadens, while the radiative rate remains roughly constant. This implies that the gate tunability of the refractive index or dielectric function is primarily dictated by non-radiative decay mechanisms. On resonance, the dielectric function in eq 2 diverges as $\gamma_{nr} \to 0$, suggesting that, by suppressing the non-radiative pathways in the system, we can potentially achieve even larger refractive index modulation. While the index modulation has not been reported, previous reports have demonstrated narrow reflectance line widths, approaching the homogeneous line width limit, where $\gamma_{nr} \ll \gamma_r$.[24,25,40] We believe even larger tunability can be achieved using these near-homogeneous line width heterostructures that are optimized to observe the coherence properties of $MoSe_2$.

CONCLUSIONS

In summary, we show remarkable tunability in the complex refractive index of $MoSe_2$ at both the A and B exciton energies, highlighting its potential for use as a reconfigurable active element in optoelectronic systems, including modulators and active metasurfaces. We find that both temperature and Fermi level modulation leads to an ENZ behavior, resulting in a transition from dielectric to metallic, accompanied by large changes in reflectance amplitude and phase. The large permittivity and index modulation result from Pauli-blocking, Coulomb scattering, and screening, which directly influence the radiative and non-radiative channels, oscillator strengths, and resonance line widths. Our findings of large electrical tunability provide a route for exploring novel phenomena and device applications based on monolayer TMDC excitons.

ASSOCIATED CONTENT

Supporting Information

The Supporting Information is available free of charge at https://pubs.acs.org/doi/10.1021/acs.nanolett.1c02199.

Additional experimental and simulation details, materials, and methods, including Figures S1−S13 with fringe images and interferometry data (PDF)

AUTHOR INFORMATION

Corresponding Author

Harry A. Atwater − *Thomas J. Watson Laboratory of Applied Physics, California Institute of Technology, Pasadena, California 91125, United States;* orcid.org/0000-0001-9435-0201; Email: haa@caltech.edu

Authors

Melissa Li − *Thomas J. Watson Laboratory of Applied Physics, California Institute of Technology, Pasadena, California 91125, United States;* orcid.org/0000-0003-1534-4191

Souvik Biswas − *Thomas J. Watson Laboratory of Applied Physics, California Institute of Technology, Pasadena, California 91125, United States*

Claudio U. Hail − *Thomas J. Watson Laboratory of Applied Physics, California Institute of Technology, Pasadena, California 91125, United States*

Complete contact information is available at: https://pubs.acs.org/10.1021/acs.nanolett.1c02199

Author Contributions

M.L, S.B., and H.A.A. conceived the project. M.L. fabricated the samples with support from S.B. M.L., S.B., and C.U.H. worked on measurements. M.L. and C.U.H. performed FDTD simulations. M.L. analyzed the data and wrote the manuscript. H.A.A. supervised the project. All authors discussed the implications of the results and provided important feedback.

Funding

The authors gratefully acknowledge support from the U.S. Department of Energy, Office of Science, under grant DE-FG02-07ER46405. C.U.H. acknowledges support from the Swiss National Science Foundation through the Early Postdoc Mobility Fellowship, grant no. P2EZP2_191880.

Notes

The authors declare no competing financial interest.

ACKNOWLEDGMENTS

The authors thank Cora Went, Joeson Wong, and Hamidreza Akbari for fruitful discussions and feedback on the work.

REFERENCES

(1) Butler, S. Z.; et al. Progress, Challenges, and Opportunities in Two-Dimensional Materials Beyond Graphene. *ACS Nano* **2013**, *7*, 2898−2926.

(2) Wang, Q. H.; Kalantar-Zadeh, K.; Kis, A.; Coleman, J. N.; Strano, M. S. Electronics and optoelectronics of two-dimensional transition metal dichalcogenides. *Nat. Nanotechnol.* **2012**, *7*, 699−712.

(3) Mak, K. F.; Lee, C.; Hone, J.; Shan, J.; Heinz, T. F. Atomically Thin ${\mathrm{MoS}}_{2}$: A New Direct-Gap Semiconductor. *Phys. Rev. Lett.* **2010**, *105*, 136805.

(4) Moody, G.; et al. Intrinsic homogeneous linewidth and broadening mechanisms of excitons in monolayer transition metal dichalcogenides. *Nat. Commun.* **2015**, *6*, 8315.

(5) Splendiani, A.; et al. Emerging Photoluminescence in Monolayer MoS2. *Nano Lett.* **2010**, *10*, 1271−1275.

(6) Stier, A. V.; Wilson, N. P.; Clark, G.; Xu, X.; Crooker, S. A. Probing the Influence of Dielectric Environment on Excitons in Monolayer WSe2: Insight from High Magnetic Fields. *Nano Lett.* **2016**, *16*, 7054−7060.

(7) Stier, A. V.; et al. Magnetooptics of Exciton Rydberg States in a Monolayer Semiconductor. *Phys. Rev. Lett.* **2018**, *120*, 57405.

(8) Raja, A.; et al. Coulomb engineering of the bandgap and excitons in two-dimensional materials. *Nat. Commun.* **2017**, *8*, 15251.

(9) Aslan, O. B.; Deng, M.; Heinz, T. F. Strain tuning of excitons in monolayer ${\mathrm{WSe}}_{2}$. *Phys. Rev. B: Condens. Matter Mater. Phys.* **2018**, *98*, 115308.

(10) Lloyd, D.; et al. Correction to Band Gap Engineering with Ultralarge Biaxial Strains in Suspended Monolayer MoS2. *Nano Lett.* **2019**, *19*, 7548.

(11) Olivieri, A.; et al. Plasmonic Nanostructured Metal−Oxide−Semiconductor Reflection Modulators. *Nano Lett.* **2015**, *15*, 2304−2311.

(12) Park, J.; et al. Electrically Tunable Epsilon-Near-Zero (ENZ) Metafilm Absorbers. *Sci. Rep.* **2015**, *5*, 15754.

(13) Jun, Y. C.; et al. Epsilon-Near-Zero Strong Coupling in Metamaterial-Semiconductor Hybrid Structures. *Nano Lett.* **2013**, *13*, 5391−5396.
(14) Dabidian, N.; et al. Electrical Switching of Infrared Light Using Graphene Integration with Plasmonic Fano Resonant Metasurfaces. *ACS Photonics* **2015**, *2*, 216−227.
(15) Yao, Y.; et al. Broad Electrical Tuning of Graphene-Loaded Plasmonic Antennas. *Nano Lett.* **2013**, *13*, 1257−1264.
(16) Hail, C. U.; Michel, A.-K. U.; Poulikakos, D.; Eghlidi, H. Optical Metasurfaces: Evolving from Passive to Adaptive. *Adv. Opt. Mater.* **2019**, *7*, 1801786.
(17) Huang, Y.-W.; et al. Gate-Tunable Conducting Oxide Metasurfaces. *Nano Lett.* **2016**, *16*, 5319−5325.
(18) Shirmanesh, G. K.; Sokhoyan, R.; Wu, P. C.; Atwater, H. A. Electro-optically Tunable Multifunctional Metasurfaces. *ACS Nano* **2020**, *14*, 6912−6920.
(19) Kafaie Shirmanesh, G.; Sokhoyan, R.; Pala, R. A.; Atwater, H. A. Dual-Gated Active Metasurface at 1550 nm with Wide (>300°) Phase Tunability. *Nano Lett.* **2018**, *18*, 2957−2963.
(20) Yu, Y.; et al. Giant Gating Tunability of Optical Refractive Index in Transition Metal Dichalcogenide Monolayers. *Nano Lett.* **2017**, *17*, 3613−3618.
(21) Zhou, Y.; et al. Probing dark excitons in atomically thin semiconductors via near-field coupling to surface plasmon polaritons. *Nat. Nanotechnol.* **2017**, *12*, 856−860.
(22) Ajayi, O. A; et al. Approaching the intrinsic photoluminescence linewidth in transition metal dichalcogenide monolayers. *2D Mater.* **2017**, *4*, 031011.
(23) Cadiz, F.; et al. Excitonic Linewidth Approaching the Homogeneous Limit in ${\mathrm{MoS}}_{2}$-Based van der Waals Heterostructures. *Phys. Rev. X* **2017**, *7*, 21026.
(24) Scuri, G.; et al. Large Excitonic Reflectivity of Monolayer ${\mathrm{MoSe}}_{2}$ Encapsulated in Hexagonal Boron Nitride. *Phys. Rev. Lett.* **2018**, *120*, 37402.
(25) Back, P.; et al. Realization of an Electrically Tunable Narrow-Bandwidth Atomically Thin Mirror Using Monolayer ${\mathrm{MoSe}}_{2}$. *Phys. Rev. Lett.* **2018**, *120*, 37401.
(26) van de Groep, J.; et al. Exciton resonance tuning of an atomically thin lens. *Nat. Photonics* **2020**, *14*, 426−430.
(27) Datta, I.; et al. Low-loss composite photonic platform based on 2D semiconductor monolayers. *Nat. Photonics* **2020**, *14*, 256−262.
(28) Dean, C. R.; et al. Boron nitride substrates for high-quality graphene electronics. *Nat. Nanotechnol.* **2010**, *5*, 722−726.
(29) Wang, Z.; Zhao, L.; Mak, K. F.; Shan, J. Probing the Spin-Polarized Electronic Band Structure in Monolayer Transition Metal Dichalcogenides by Optical Spectroscopy. *Nano Lett.* **2017**, *17*, 740−746.
(30) Sidler, M.; et al. Fermi polaron-polaritons in charge-tunable atomically thin semiconductors. *Nat. Phys.* **2017**, *13*, 255−261.
(31) Ross, J. S.; et al. Electrical control of neutral and charged excitons in a monolayer semiconductor. *Nat. Commun.* **2013**, *4*, 1474.
(32) Qiu, D. Y.; da Jornada, F. H.; Louie, S. G. Optical Spectrum of ${\mathrm{MoS}}_{2}$: Many-Body Effects and Diversity of Exciton States. *Phys. Rev. Lett.* **2013**, *111*, 216805.
(33) Gao, S.; Liang, Y.; Spataru, C. D.; Yang, L. Dynamical Excitonic Effects in Doped Two-Dimensional Semiconductors. *Nano Lett.* **2016**, *16*, 5568−5573.
(34) Van Tuan, D.; et al. Probing many-body interactions in monolayer transition-metal dichalcogenides. *Phys. Rev. B: Condens. Matter Mater. Phys.* **2019**, *99*, 85301.
(35) Goldstein, T. Ground and excited state exciton polarons in monolayer MoSe2. *J. Chem. Phys.* **2020**, *153*, 071101.
(36) Li, Y.; et al. Measurement of the optical dielectric function of monolayer transition-metal dichalcogenides: ${\mathrm{MoS}}_{2}$, $\mathrm{Mo}\mathrm{S}{\mathrm{e}}_{2}$, ${\mathrm{WS}}_{2}$, and $\mathrm{WS}{\mathrm{e}}_{2}$. *Phys. Rev. B: Condens. Matter Mater. Phys.* **2014**, *90*, 205422.
(37) Kravets, V. G.; et al. Measurements of electrically tunable refractive index of MoS2 monolayer and its usage in optical modulators. *npj 2D Mater. Appl.* **2019**, *3*, 36.
(38) Hsu, C.; et al. Thickness-Dependent Refractive Index of 1L, 2L, and 3L MoS2, MoSe2, WS2, and WSe2. *Adv. Opt. Mater.* **2019**, *7*, 1900239.
(39) Sherrott, M. C.; et al. Anisotropic Quantum Well Electro-Optics in Few-Layer Black Phosphorus. *Nano Lett.* **2019**, *19*, 269−276.
(40) Zhou, Y.; et al. Controlling Excitons in an Atomically Thin Membrane with a Mirror. *Phys. Rev. Lett.* **2020**, *124*, 27401.

https://doi.org/10.1021/acs.nanolett.1c02199
Nano Lett. XXXX, XXX, XXX−XXX